Influence of the road texture anisotropy on the noise radiated by a slick tyre

Philippe Klein

Influence of the road texture anisotropy on the noise radiated by a slick tyre

P. Klein

Ifsttar, 25, avenue François Mitterrand, 69675 Bron, France
philippe.klein@ifsttar.fr

The road texture is known to play a fundamental role in the tyre/road noise generation. Bi-dimensional profiles are often used to evaluate the performances of road surfaces as regards the rolling noise emission. In order to predict noise levels from bi-dimensional longitudinal texture profiles, assumptions concerning the three-dimensional distribution properties of the road surface are required. If these assumptions are not met, a deviation may occur in noise level evaluations.

This paper aims to provide an insight into the expected radiated noise level variability due to possible texture anisotropy in the case of a slick tyre. The approach used in this paper is based on simulation tools intended to provide texture and noise data, which are statistically analyzed afterwards. Three-dimensional gaussian random texture fields are numerically generated from a known bi-dimensional texture power spectral density assuming elliptical anisotropy. These texture fields are used as input of a dynamic rolling model that provides the radial vibration of the tyre belt. The resulting radiated noise levels are evaluated with a BEM model. The relationships obtained between the elliptical anisotropy rating and the calculated noise levels are presented and discussed.

1   Introduction

Road texture is known to play a fundamental role in the tyre/road noise generation so long as the tyre tread pattern is not too aggressive. Its influence has previously been shown through empirical relationships between texture and noise levels evaluated from measured data [1]. Other studies have pointed out that the global trend between texture and noise levels obtained on transversely textured road surfaces are very different from those obtained on road surfaces that present randomly distributed textures [2, 3].

Hybrid approaches have been developed to improve the accuracy of prediction tools; they mix statistical laws and simplified physical models. Prediction tools that use bi-dimensional texture profiles as input to evaluate the performance of a road surface are limited in their field of validity. Statistical relationships fitted to quasi-isotropic texture would not apply to transverse texture.

This paper aims to investigate the possible variability due to anisotropy that may occur while trying to evaluate the noise radiated by a slick tyre from 2D profile considering the road texture as isotropic although it is not. The adopted approach is based on simulation tools intended to provide texture and noise data which are statistically analyzed afterwards. Three-dimensional gaussian random texture fields are numerically generated from a known bi-dimensional texture power spectral density assuming elliptical anisotropy. These texture fields are used as input of a dynamic rolling model that provides the radial vibration of the tyre belt. The resulting radiated noise levels are evaluated with a BEM model.

The first part of the paper describes the physical model that provides the noise data from the texture input. A second part deals with the generation of 3D texture samples used as input of the noise prediction model and the way the anisotropy is introduced. In the third part, the adopted simulation plan is presented. The results are presented in the fourth part.

2   Noise prediction model

The model used for evaluating the noise levels from the texture input is the DySiRoN model (Dynamic Simulation of Rolling Noise). It aims to evaluate the noise produced by the the radial vibration of the tyre rolling on a rough surface (this model does not take into account the air-pumping phenomenon). It consists of several sub-models. The core is based on the dynamic rolling model suggested by Kropp [4]. The tyre belt is represented by an orthotropic rectan-

gular plate laying on an elastic foundation. Its behaviour is governed by physical parameters [5]: the plate stiffness, its tension due to the inflation pressure, the internal air stiffness and all associated loss factors. The tyre rubber is modeled by independent springs with constant stiffness (the value used here is 500 MN/m^3). Only the compression of the springs is allowed. The contact forces are evaluated in the time domain in order to allow the consideration of local non contact instances. An illustration of the contact force distribution at one given moment is drawn in Figure 3. The discretization step in the lateral and longitudinal dimension is approximately 4 mm. Once the contact forces have been evaluated, the radial velocity components are determined in the frequency domain.
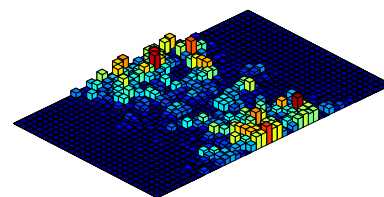

Figure 1: Normal force distribution in the contact zone.

The model is supplemented by a BEM model indented to evaluate the noise emission produced by the radial vibration of the tyre belt in the presence of a perfectly reflecting surface. Therefore the horn effect is taken into account. The gap between the bottom of the tyre and the reflecting surface was set at 1 mm. The wheel geometry (made of the tyre belt and a simplified rim) and the quadrangular mesh used is represented in Figure 2. As can be observed, the mesh is refined near the contact zone due to the proximity of the reflecting surface. The vibration at the nodes is obtained by projection of the rectangular plate on the actual wheel shape. The velocity at the rim is set to zero.

Considering the chosen time interval used in the simulation, the BEM model allows the evaluation of several noise related quantities for frequencies up to 3 kHz as narrow band spectra.

3   Generation of texture surfaces

The method used to generate texture surfaces has been suggested in [6]. It enables the generation of gaussian random surfaces from the 2D Power Spectral Density assuming that the surface is isotropic. This method has been extended
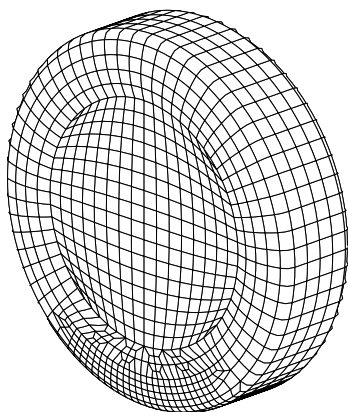
Figure 2: Quadrangle surface meshing of the wheel.

to introduce simple anisotropy conditions that can be qualified by an anisotropy rating.

3.1 Generation of isotropic surfaces

The generation of gaussian random surfaces is performed in several stages. The input data required is the 2D autocorrelation function which can be directly evaluated from 2D texture profiles or calculated by inverse Fourier transform from a known 2D Power Spectral Density (PSD) $S_z(\nu)$ where ν is the spatial frequency.

Let $R_z(u)$ be this 2D autocorrelation function. In the case where a perfect isotropy is considered, the corresponding 3D autocorrelation function $R_Z(u, v)$ is obtained by rotating the 2D autocorrelation around the origin:

$$C_Z(u, v) = C_z\left(\sqrt{u^2 + v^2}\right).$$

Once the 3D autocorrelation evaluated, the 3D Power Spectral Density $S_Z(\mu, \nu)$ is calculated using the Fourier transform. The phases of the Fourier components $\sqrt{S_Z}$ are randomized and a surface is generated using the inverse Fourier transform. As described in [7], the phases are associated by pairs to ensure that the generated surface keeps real values.

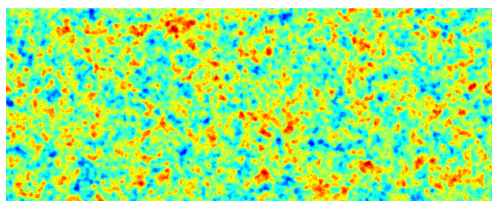An example of isotropic surface seen from the top is given in Figure 3:

Figure 3: Example of an isotropic surface.

3.2 Introduction of elliptical anisotropy

Elliptical anisotropy is introduced in the process described above by modifying the construction of the 3D autocorrelation function. It is also obtained by rotating the 2D autocorrelation function but introducing a dilatation or compression in a chosen direction defined by the angle θ_0 with respect to the rolling direction. This dilatation is controlled by the ellipse

represented in Figure 4. It is constructed so as to have no expansion nor compression in the rolling direction in order to keep a fixed PSD in this direction.
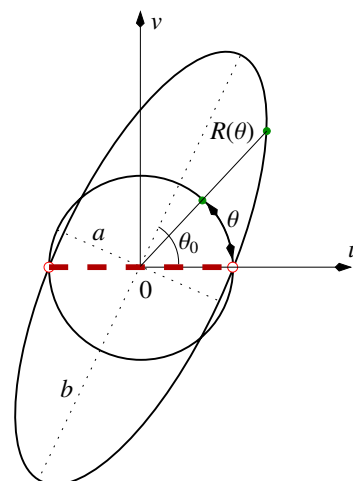

Figure 4: Ellipse definition (u: rolling direction - v: transverse direction)

If we note R_d the anisotropy rating (the elongation of the ellipse or the ratio between the long axis b and the small axis a), the expansion for fixed values of R_d and θ_0 is given as a function of the angle $\theta(u, v)$ ($\tan\theta = v/u$):

$$R(\theta) = \sqrt{\frac{R_d^2 \cos^2(\theta - \beta) + \sin^2(\theta - \beta)}{R_d^2 \cos^2\beta + \sin^2\beta}},$$

with $\beta = \arctan(R_d \tan\theta_0)$. The corresponding $R_Z(u, v)$ function is defined by:

$$C_Z(u, v) = C_z\left(\frac{\sqrt{u^2 + v^2}}{R(\theta(u, v))}\right).$$

Once $R_Z(u, v)$ is defined, the subsequent stages previously described for the isotropic condition are applied to obtain a surface with the desired parameters. Examples of generated anisotropic surfaces are shown in Figure 5.
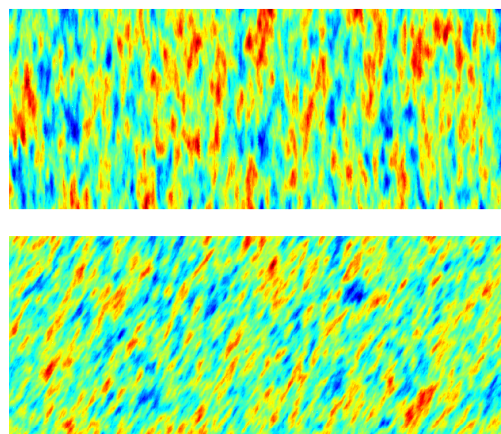

Figure 5: Anisotropic surfaces generated with $R_d = 4$, $\theta_0 = \pi/2$ (top), $R_d = 3$, $\theta_0 = \pi/3$ (bottom)

4 Simulation plan

4.1 Texture data

The experimental plan has been defined to provide quite a large set of data. 2D profiles measured on 3 different road surfaces (which will be denoted A, B, and C) have been used to estimate their respective bidimensional PSD. These PSD have been smoothed to provide associated templates. These templates are constructed as continuous piecewise functions with the form (see [8]):

$$S(v) = S(v_i)\left(\frac{v}{v_i}\right)^{-\alpha_i} ,$$

for $v_i \le v < v_{i+1}$, with $i = 1$ to $i = n - 1$.

The continuity between adjacent intervals is ensured by the following condition:

$$S(v_{i+1}) = S(v_i)\left(\frac{v_{i+1}}{v_i}\right)^{-\alpha_i} ,$$

The three measured PSD and resulting templates are shown Figure 6. These templates have been used to determine the corresponding 2D autocorrelation functions. The rms values of templates A, B and C are respectively 0.8 mm, 1.7 mm and 2.3 mm.
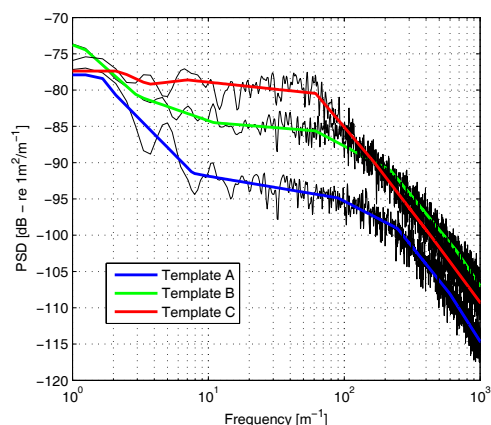

Figure 6: 2D PSD and associated templates evaluated from 2D measured texture profiles (black thin line: PSD - colored thick lines: templates).

3D texture fields have been generated from the templates according to the method described in part 3.2. The first set of textures is built from the three templates considering transverse anisotropy with a fixed orientation $\theta_0 = \pi/2$ and a number of R_d values: $R_d = 0.25, 0.5, 1$ (isotropic reference), 2, 3, 4, 6 and 8. Additional configurations have been considered for template A introducing several orientations with angle values $\theta_0 = \pi/3$ and $\pi/4$.

Some of the corresponding ellipses are represented in Figure 7.

4.2 Noise data

The simulations have been performed for a rolling speed $V = 80$ km/h. 16 m long sections were generated; the last 8 meters of each generated surface were used to evaluate the noise levels (one evaluation performed per approximately 2 m long tyre revolution and averaged over 4 revolutions).
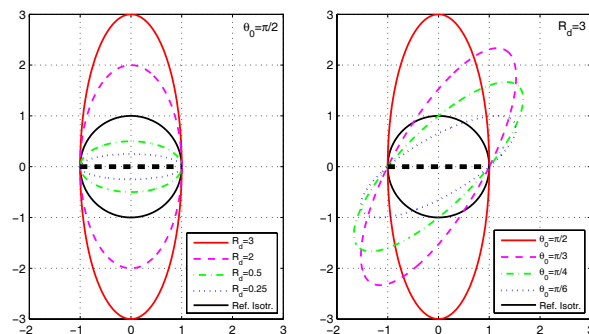

Figure 7: Some of the anisotropy configurations of the simulation plan.

The noise data have been calculated as third-octave band or A-weighted global levels from the narrow band spectra. These quantities are

- the total radiated acoustic power, L_W

- the acoustic pressure at the French CPX standard lateral and trailing microphone positions L_{Pcpx}(see Figure 8).
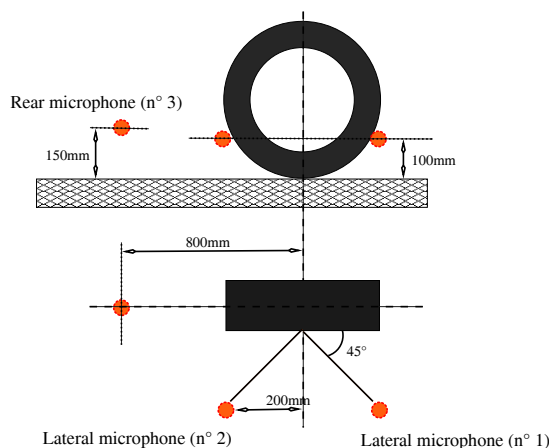

Figure 8: CPX microphone positions of the French CPX measurement system

5 Results

This part provides an overview of the simulation results. In these results the isotropic cases ($R_d = 1$) are used as reference cases.

5.1 Influence of the elliptical anisotropy on the total radiated power

The calculated total radiated power third-octave noise levels L_{Wiso} corresponding to the isotropic surfaces generated from the three templates are represented in Figure 9.

The difference $L_W - L_{Wiso}$ in terms of third-octave levels for $\theta_0 = \pi/2$ is represented as a function of R_d in Figure 10 (top graph) for template A. Similar trends are obtained with templates B and C. The global trend is the progressive increase of the third-octave levels as R_d increases. The
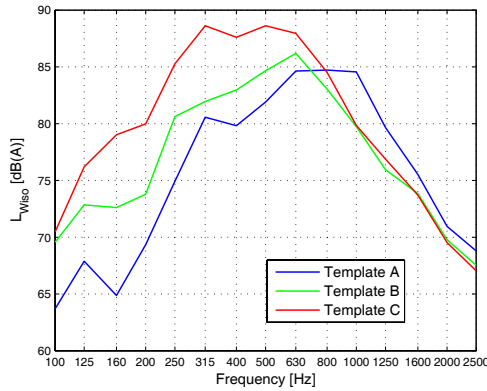
Figure 9: Radiated power third-octave levels for the isotropic surfaces obtained from templates A, B and C
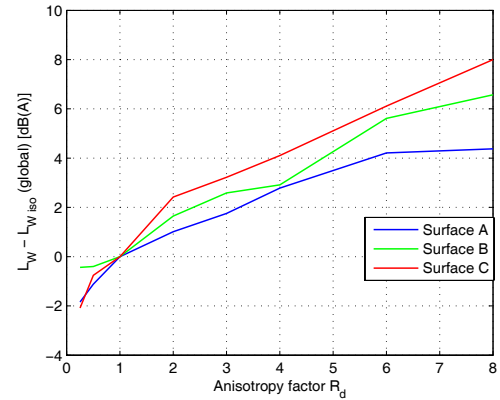

Figure 11: Global radiated power dB(A) level differences with respect to the isotropic surface as a function of R_d
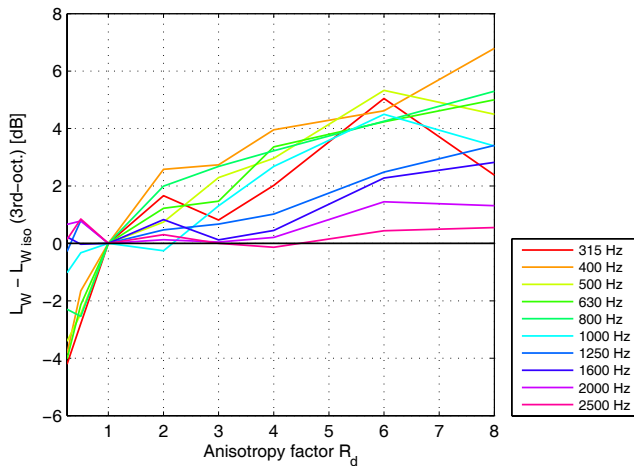

Figure 10: Radiated power level differences with respect to the isotropic surface as a function of R_d - Third-octave bands (surface A)
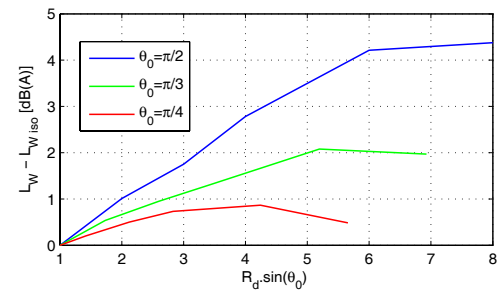

Figure 12: Global radiated power dB(A) level differences with respect to the isotropic surface as a function of $R_d \sin \theta_0$

levels, specifically on the average level of both lateral microphone positions. Similar results have been obtained as shown in Figures 13 and 14.
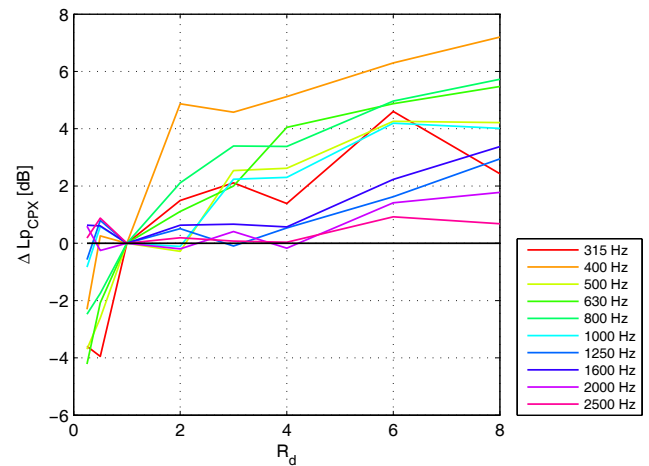
amount of this increase depends on the frequency considered. It reaches 6 dB at 400 Hz for $R_d = 8$.

The corresponding differences in terms of global dB(A) power levels are given in Figure 11 for the three templates. For $R_d < 1$, the global radiated power is lower than the one obtained for the isotropic case. On the other hand, for $R_d > 1$ it is higher than for the reference case and gradually increases with growing R_d values. The differences reach rather high levels. The lowest values are observed for template A which show the lower texture levels. The highest values are observed for template C which presents the highest texture levels while intermediate values are obtained for template B.

Additional results have been obtained introducing a rotation of the elliptical anisotropy with respect to the transverse direction. The differences obtained for template A are drawn in figure 12 as a function of the quantity $R_d \sin \theta_0$ which includes a correction for the angular orientation of the anisotropy. As observed, the angular orientation produces a noise level reduction with respect to the transverse orientation ($\theta_0 = \pi/2$).

5.2 Influence of the elliptical anisotropy on CPX levels

To supplement the results obtained on the total radiated power, the same evaluations have been performed on CPX

Figure 13: Radiated power level differences with respect to the isotropic surface as a function of R_d - Third-octave bands (surface A)

5.3 Relationship between total force and radiated power variations

The observed increase in noise levels as the R_d rating increases can be explained by the stronger transverse correlation between parallel longitudinal profiles, producing more or less in-phase excitation of the tyre which results in higher tyre vibration levels.
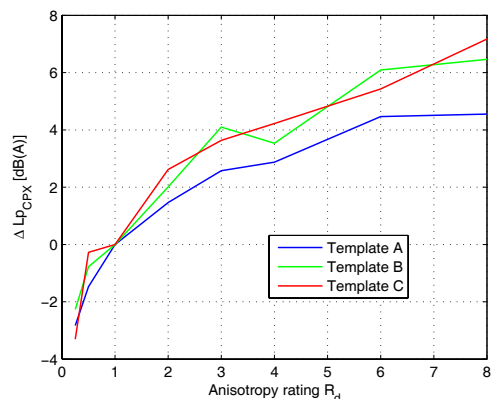
Figure 14: CPX global dB(A) level differences with respect to the isotropic surface as a function of R_d rating
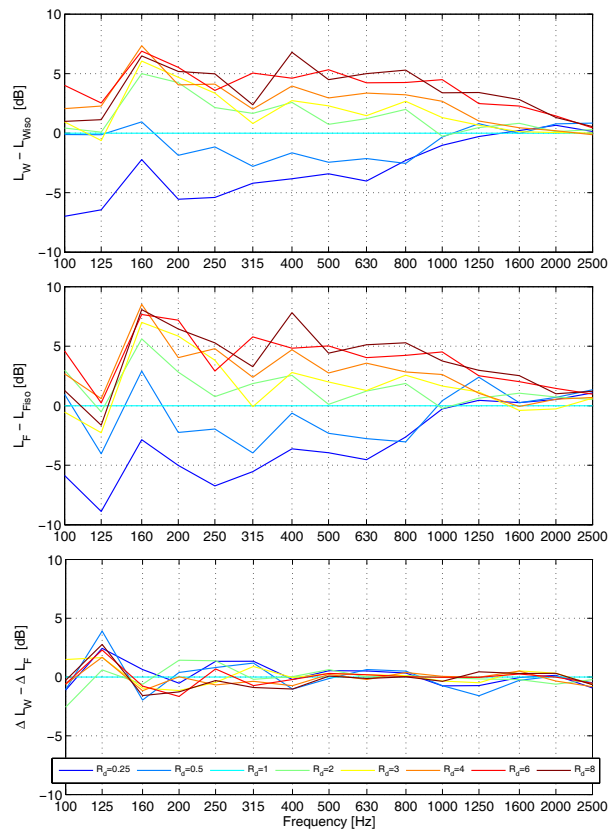

Figure 15: Differences $\Delta L_W(R_d, f)$ (top graph), $\Delta F(R_d, f)$ (middle graph) and $\Delta L_W(R_d, f) - \Delta F(R_d, f)$ (bottom graph) obtained for template A

Further investigations have been undertaken concerning the relationship between the noise radiated power and the contact forces evaluated in the rolling model simulations. Similar investigations also based on data obtained by simulations were previously presented in [9] and showed that the radiated power level L_W is rather highly correlated with the level of total normal force acting on the tyre belt (which will be denoted as L_F). The top and middle graphs of the Figure 15 show the differences between the anisotropic surface and the isotropic surface in terms of noise radiated power 1/3−oct levels $\Delta L_W(R_d, f) = L_W - L_{Wiso}$ and total force 1/3−oct levels $\Delta L_F(R_d, f) = L_F - L_{Fiso}$ as a function of the frequency for different R_d values (transverse texture orientation $\theta_0 = \pi/2$). Both graphs show a strong influence of the R_d rating depending on the frequency considered. Considering the difference $\Delta L_W(R_d, f) - \Delta L_F(R_d, f)$ drawn in the bottom graph of the Figure 15, most of the radiated power variations with respect to the isotropic case seem to be explained by the variations of the global force acting on the tyre belt.

6 Conclusion

Investigations performed to address the influence of road texture anisotropy have been presented in this paper. They are based on simulation results obtained from synthetised texture data with a dynamic rolling model coupled with a BEM model providing tyre belt radial vibration induced noise levels. Quite simple "elliptical" anisotropy conditions have been considered. The results show that this elliptical anisotropy may lead to relatively large global noise level differences between surfaces presenting the same longitudinal texture spectrum but not the same isotropy properties. The relationship between the total normal force applied on the tyre belt and the radiated noise has been highlighted.

References

[1] U. Sandberg, G. Descornet, "Road surface influence on tire/road noise", *INTER-NOISE*, Miami (1980)

[2] P.G. Abbott, S. Philips, "Vehicle noise derived from the statistical pass-by method and road surface texture", *NOISE-CON*, Seattle, Washington (1996)

[3] J.F. Hamet, P. Klein, "Use of a rolling model for the study of the correlation between road texture and tire noise", *INTER-NOISE*, The Hague, The Netherlands (2001)

[4] W. Kropp, "Ein Model zur Beschreibung des Rollgeräusches eines unprofilierten Gürtelreifens auf rauher Strassenoberfläche", *PhD Thesis* (1992)

[5] J.F. Hamet, "Tire/road noise: time domain green's function for the orthotropic plate model", *Acta Acustica united with Acustica* **87**, 470-474 (2001)

[6] D. Cebon, D.E. Newland, "The artificial generation of road surface topography by the inverse FFT method", *Proceedings of the Xth Symposium on the Dynamics of Vehicles on Roads and on Railway Tracks*, Cambridge , 23-49 (1985)

[7] J.J. Wu, "Simulation of rough surfaces with FFT", *Tribology International* **33**, 47-58 (2000)

[8] C.J. Dodds, J.D. Robson, "The desciption of road surface roughness", *Journal of Sound and Vibration* **31**(2), 175-183 (1973)

[9] P. Klein, J.F. Hamet, "The correlations between texture related quantities and the tyre radiated noise levels evaluated from a dynamic rolling model", *Euronoise*, Tampere, Finland (2006)